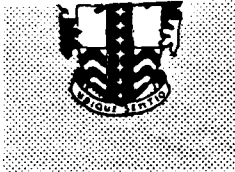UNLIMITED

②

AD-A242 201

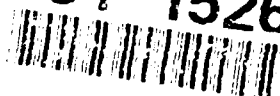# RSRE
MEMORANDUM No. 4464

ROYAL SIGNALS & RADAR ESTABLISHMENT

EXTRACTION OF SHAPE INFORMATION FROM PREDICTED IRRADIANCE PROFILES IN INFRARED IMAGES

Author: P W Foulkes

RSRE MEMORANDUM No. 4464

91-15261

UNLIMITED

ROYAL SIGNALS AND RADAR ESTABLISHMENT

Memorandum 4464

Title: Extraction of shape information from predicted irradiance profiles in infrared images

Author: P W Foulkes

Date: March 5, 1991

Summary

In this paper, we address the problem of infrared image formation and derive an irradiance equation for simple infrared scenes. We consider the complications caused by mutual illumination of one or more bodies and indicate how the infrared irradiance equation can also be specified for more complex scenes.

The infrared irradiance equation we derive is solved in closed form for some simple geometries for both Lambertian and non-Lambertian surfaces. Experimental results from a variety of scene geometries compare favourably with the theoretically derived equations, indicating the validity of the theoretical analysis.

We describe how a knowledge of the formation of infrared images can be used to predict the image irradiance pattern of a particular object. We also show how, with a knowledge of the radiance properties and surface geometry of the object, it is possible to detect instances of that object in a scene.

Examples of successful object detection based on an understanding of the image irradiance are presented.

Contents

1 Introduction

All bodies whose temperatures are above absolute zero emit energy. For bodies at or around room temperature, the majority of the energy emitted by the body will be emitted in the infrared part of the electromagnetic spectrum, as heat. Wien's Displacement law predicts that for a body at 300K, the wavelength of the peak in the transmitted radiation is approximately 9.7μ. Radiation at this frequency is not greatly affected by the atmosphere for ranges less than a few miles and so can be used to detect the presence of the object emitting the radiation. Since bodies emit infrared energy in the absence of light, infrared imagers can be used to detect their presence when normal visual imagers would fail. There are clearly very good reasons for researching infrared imagers.

A black body is defined as a complete absorber of energy and the most effective radiator of energy. No real body behaves as a black body across the entire spectrum, though certain materials approach "blackness" over limited ranges of the spectrum.

Lambert proposed that the radiation coming from a diffusely radiating body is highest in the direction of the surface normal of the body and falls off in proportion to the cosine of the angle from the normal in other viewing directions. Lambert's law, which expresses this mathematically is only valid for perfect diffusers, but serves as a useful tool for analysing approximately black surfaces.

A consequence of Lambert's law is that a true diffuse emitter appears equally bright from all view directions. This is because when viewed at an angle θ from the surface normal, the apparent area of a surface patch is *foreshortened* by a factor $cos(\theta)$. The energy emitted in the direction θ is, from Lambert's law $cos(\theta)$ times the energy emitted in the direction of the surface normal. The perceived brightness is the same, therefore, since the amount of energy being radiated from a perceived unit area is equal. This means that an intensity profile of a uniform temperature warm convex object will indicate equal radiance across the surface. This has significant consequences which will be discussed later.

2 Radiation transfer

In considering the effect of radiation from one object to another or from an object to an imager, we need first to develop an equation relating the radiated energy transmitted from an element of one surface patch to an element of another surface patch when the two surfaces are at arbitrary orientations in space. In principle we can then calculate the radiant energy from any body to any other body by integrating the elemental radiances over the surfaces of the bodies.

Consider the elemental surface patches dS_1 and dS_2 of the two surfaces S_1 and S_2 depicted in figure 1. The line joining the elemental surface patches is of length r and makes an angle θ_1 with the normal from dS_1 and an angle θ_2 with the normal from dS_2. When looking from point 1, the centre of the surface patch dS_1, the patch dS_2 subtends a solid angle $d\omega_2$, where $d\omega_2 = \frac{dS_2 cos(\theta_2)}{r^2}$. Following Stefan-Boltzmann, the radiant power emitted by dS_1 which is incident on element dS_2 is given by $dW_1 = \epsilon_1 \sigma T_1^4 cos(\theta_1)dS_1 d\omega_2$, where T_1 is the absolute temperature of S_1 and ϵ_1 is the emissivity of S_1. Substituting for $d\omega_2$, we have:

$$dW_1 = \frac{\epsilon_1 \sigma T_1^4}{r^2}cos(\theta_1)cos(\theta_2)dS_1 dS_2 \qquad (1)$$

Integrating over the surface S_2, we find that the irradiation on the surface S_2 due to the surface patch dS_1 is

$$W_1 = \epsilon_1 \sigma T_1^4 dS_1 \int_{S_2} \frac{cos\,\theta_1 cos\,\theta_2}{r^2}dS_2 \qquad (2)$$

The term "view factor" or "geometrical factor" of the surface S_2 from the surface S_1 is given to the integral: $F_{12} = \int_{S_2} \frac{cos\,\theta_1 cos\,\theta_2}{r^2}dS_2$. Substituting F_{12} into equation 2 gives $W_1 = \epsilon_1 \sigma T_1^4 dS_1 F_{12}$. The integral F_{12} can only be evaluated explicitly for simple geometric shapes. Integrating over the surface S_1 and assuming that the surfaces are opaque (and hence that absorptivity equals emissivity), we have the total power absorbed by surface S_2 radiated by surface S_1:

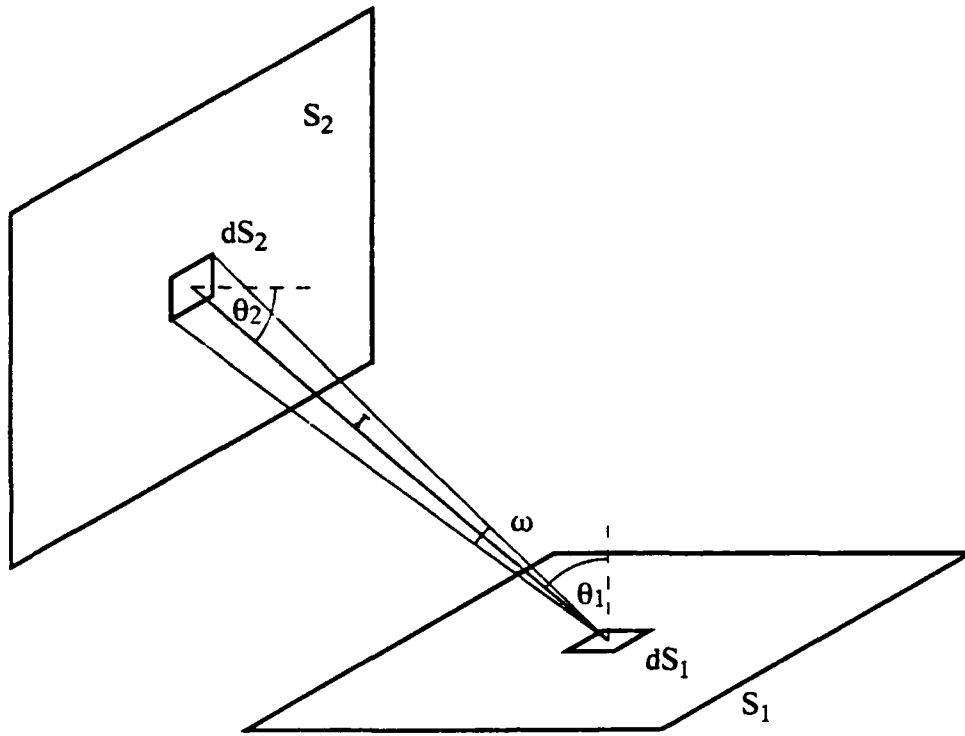$$W_{12} = \epsilon_1 \epsilon_2 \sigma T_1^4 \int_{S_1} F_{12}dS_1$$

Figure 1: Exchange of radiated energy between two surfaces

3 Self irradiation

Consider now the effect of radiation of one part of a body affecting another part of the same body. This will occur whenever a body has concavities. As stated in the previous section, it is not possible to obtain explicit solutions for the view factor unless the geometry of the problem is quite simple. Here we begin by analysing a manageable problem: that of a concave semi-cylinder emitting radiation equally in all directions.

Figure 2 shows a section of a concave semi-cylinder viewed in the direction indicated. From the geometry of the cylinder, we note that the angle between the surface normal of element dS_1 and the line joining dS_1 to dS_2 is also equal to ϕ. We make the reasonable assumption that emissivity is constant in the cylinder and we will assume that the temperature of the cylinder is constant throughout. The general problem described in the previous section is thus greatly simplified.

The distance d between point 1 and point 2 can be calculated by considering the geometry of the figure: $d = 2r\cos\phi$. As was the case in the previous section, the solid angle subtended by the patch dS_2 is given by $d\omega_2 = \frac{dS_2\cos\phi}{d^2}$. Substituting for d, we get $d\omega_2 = \frac{dS_2}{4r^2\cos\phi}$. The radiant power emitted by dS_1 for the general case is given by equation 1. Making the relevant changes for this specific case, we have:

$$dW_1 = \frac{\epsilon\sigma T^4}{4r^2}dS_1 dS_2. \tag{3}$$

We notice that dW_1 is not dependent on either θ or ϕ. To calculate the total irradiance at S_2 simply involves integrating with respect to α for $0 \leq \alpha \leq \pi$.

Now consider the hypothetical case of a cylinder which is a Lambertian emitter but a spectral reflector of infrared irradiation. To simplify further, assume that multiple reflections do not occur. (For a real surface, this is usually not unreasonable as the thermal reflectivity of most materials is quite low.) Figure 3 shows the ray trace of two rays emanating from the wall of the cylinder and reflecting from a different part of the wall towards the viewer.

For this spectral reflection case each position on the cylinder wall reflects radiation from only one other position on the wall in the direction of the viewer. The radius at the point of reflection bisects the angle between the line of sight of the viewer and the line to the point of emission. Ray 2 is a typical example of a position on the surface of the cylinder reflecting the irradiation from another position on the surface of the cylinder.
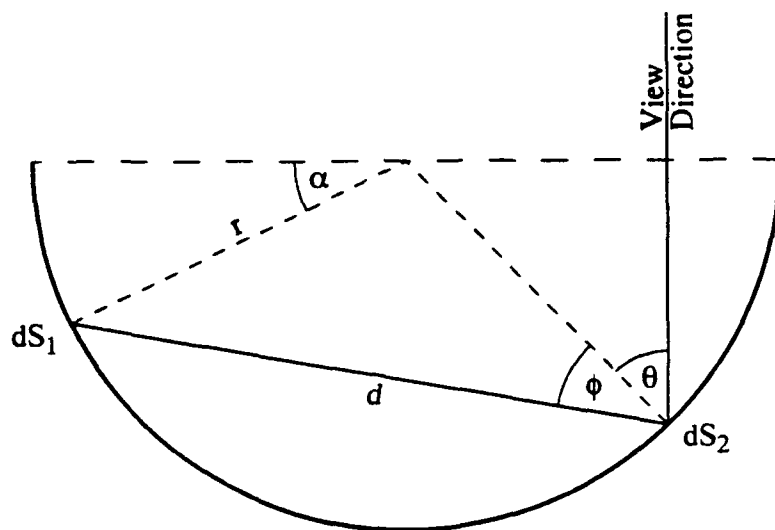
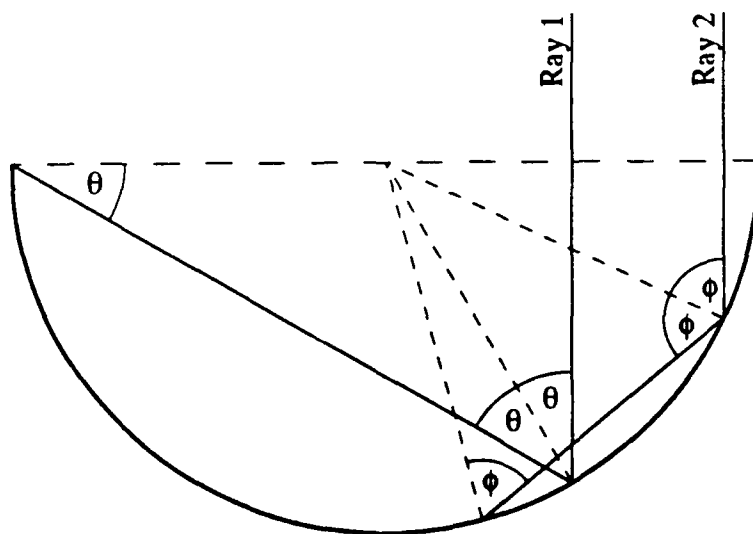Figure 2: Geometry of self-irradiation of concave cylinder

Figure 3: Geometry for specular reflection of irradiation

Figure 4: Predicted intensity profile of specularly reflecting concave non-Lambertian radiator

For a Lambertian emitter, equation 3 tells us that the magnitude of the irradiation at dS_2 (figure 2) is independent of the angle ϕ. Given that this is so, then the irradiation at the viewer due to reflection will be the same for all points on the surface of the cylinder which reflect radiation in the direction of the viewer. Not all points on the surface will reflect in the direction of the viewer, however: only points which satisfy the geometry required for reflection. In figure 3, Ray 1 illustrates the limiting case: any points nearer to the centre of the cylinder will not reflect another point on the cylinder towards the viewer. For this limiting case, θ is easily calculated as $\frac{\pi}{6}$ radians.

The reflective component of the intensity profile will have two regions of equal intensity starting at the edges of the semi-cylinder, each one quarter of the diameter of the cylinder surrounding a region with the same intensity as the background.

Consider now a body which is not a Lambertian radiator of energy. Assume that the body has a radiation distribution which has its strongest component in the direction of the surface normal with intensity of radiation dropping away rapidly in other directions. This model fits many non-black bodies. If we were viewing a convex body with this type of radiation distribution, we would expect the irradiance to reduce as the surface normal turned further away from the viewer. We will show in section 4 that certain bodies do indeed give this type of intensity profile.

In the absence of any mutual radiation effects, we would expect a concave body to have a similar intensity profile to a convex body: parts of the body's surface directed towards the viewer would appear brighter. For bodies which have radiance patterns of this type and which also exhibit reflection effects, we would expect a radiance distribution which was a superposition of the radiance distributions for the spectral reflector and the non-Lambertian emitter. This might appear similar to the intensity profile illustrated in figure 4.

For a real body, we would not expect the transition between the region in which no reflection occurs to the region in which reflection occurs to be a step as it is in the figure. The assumption that reflection of irradiation will be only in one direction is clearly unlikely to be true for real objects. If instead we postulate that the radiation will be scattered in a similar manner to the radiation pattern assumed for the non-Lambertian radiator, then the sharp corners in the expected intensity profile would be smoothed.

A model was proposed by Phong [3] for reconstructing the reflection characteristics of surfaces to generate a computer graphical representation of a surface coated with glossy white paint - a linear combination of a Lambertian component corresponding to matte white paint and a specular reflector for the lacquer cover. Horn [2] adapted the model and used it to predict the reflectivity function of a surface given the light distribution and viewing geometry. The equation used by Horn was:

$$\phi(I, E, G) = \frac{1}{2}s(n + 1)(2IE - G)^n + (1 - s)I \qquad (4)$$

where s is the fraction of incident light reflected specularly and I, E, G are the cosines of the incident i, emitted e and phase g angles respectively. The value of n determines the sharpness of the specularity peak. We will now consider how this model can be applied to the problem described above.

Consider, again using the geometry of figure 2, a non-Lambertian emitter which emits primarily in the direction normal to the surface. Let the energy emitted from dS_1 in the direction ϕ be proportional, not to $\cos(\phi)$ but to $\cos^2(\phi)$. Using the analysis leading to equation 3, we have

$$dW_1 = \frac{\epsilon\sigma T^4}{4r^2}\cos(\phi)dS_1 dS_2. \qquad (5)$$

The reflection of the ray from dS_1 at dS_2 is determined by the nature of the surface; by the incident angle ϕ; by the emitted angle θ and by the phase angle $(\phi + \theta)$ and can be approximated by equation 4. Due to the two dimensional nature of this problem, we can calculate $(2IE - G)$ quite simply:

$$2\cos\phi\cos\theta - \cos(\phi + \theta) = \cos(\phi - \theta)$$

Combining equations 4 and 5, the spectral component of the reflected beam in direction θ is given by: $\frac{1}{2}s(n+1)\cos^n(\phi-\theta)\frac{\epsilon\sigma T^4}{4r^3}\cos(\phi)dS_1 dS_2$. Integrating with respect to ϕ over the possible range of values and noticing that $dS_1 = 2rd\phi$, we get the total energy seen by the viewer from the point defined by θ due to reflection from other parts of the cylinder:

$$W_1 = s(n+1)\frac{\epsilon\sigma T^4}{4r}dS_2 \int_{\phi_1}^{\phi_2} \cos^n(\phi-\theta)\cos(\phi)d\phi \tag{6}$$

We now evaluate the integral. Substituting $y = (\phi-\theta)$ gives $\int_{y_1}^{y_2}\cos^n y \cos(y+\theta)dy$. Expanding $\cos(y+\theta)$ and tidying up, the resulting integral is given by: $\cos\theta\int_{y_1}^{y_2}\cos^{n+1}(y)dy - \sin\theta\int_{y_1}^{y_2}\cos^n(y)\sin(y)dy$. The second integral can be evaluated quite simply. Re-substituting $y = \phi - \theta$ into the solution we have:

$$\sin\theta\left[\frac{1}{1+n}\cos^{n+1}(\phi-\theta)\right]_{\phi_1}^{\phi_2} \tag{7}$$

We can get a closed form solution to the first integral for even values of n. Let $m = n/2$ and substitute $\cos^2(y) = (1-\sin^2(y))$ then the first integral is given by $\cos\theta\int_{y_1}^{y_2}(1-\sin^2(y))^m\cos(y)dy$. We now expand $(1-\sin^2(y))^m$ as a binomial: $(1-\sin^2(y))^m = \sum_{k=0}^{m}\frac{(-1)^k m!}{k!(m-k)!}\sin^{2k}(y)$. We can now integrate the expression and the solution to the first integral for even n is given by

$$\cos\theta\left[\sum_{k=0}^{m}\frac{(-1)^k m!}{k!(m-k)!}\cdot\frac{1}{2k+1}\cdot\sin^{2k+1}(\phi-\theta)\right]_{\phi_1}^{\phi_2} \tag{8}$$

(re-substituting $y = (\phi-\theta)$).

The limits for ϕ can be calculated from the geometry of the figure for the parts of the figure to the left of dS_2: $\phi_1 = \frac{\pi-2\theta}{4}$ and $\phi_2 = \frac{\pi}{2}$. Because of the way the angles were defined, it was necessary to treat the portion of the cylinder to the right of dS_2 slightly differently to the portion to the left of dS_2. The mathematics is very similar, however and will not be repeated here. The spectral reflection component of the solution of the original equation is proportional to the sum of the results of equations 7 and 8.

Calculating the non-specular reflection component is much simpler. Using equations 4 and 5; and making the substitution $dS_1 = 2rd\phi$, the non-specular component is given by: $(1-s)\frac{\epsilon\sigma T^4}{2r}dS_2\int_{\phi_1}^{\phi_2}\cos^2(\phi)d\phi$. The integral can be solved to give:

$$\left[\frac{1}{2}\phi+\frac{1}{4}\sin(2\phi)\right]_{\phi_1}^{\phi_2} \tag{9}$$

Using the same angle definitions as before, for consistency, we calculated this integral in two parts: to the left and the right of dS_2 and summed the result.

The final component of radiation reaching the viewer using this model is that which is emitted directly from the body of the cylinder. This is also simple to calculate using the radiation distribution of the surface which was defined earlier to be proportional to $\cos^2(\theta)$.

The total solution for the irradiance at the viewer was calculated. The irradiance distribution depends on the radius of the cylinder: the smaller the radius, the greater the importance of the reflected components. Figure 5 shows the irradiance profile predicted by the model described above for a unit radius with n chosen for a "fairly specular" surface (as defined by Phong).

We can see that taking account of the assumptions we made about smoothing sharp corners of the profile we anticipated from our earlier discussion, and plotted in figure 4, the two approaches would give fairly similar results: of course the first approach was only intended to give a rough guide to the shape; while the second plot depends strongly on the accuracy of the assumptions made.

We show in section 4 that intensity profiles of irradiation from non-black body concave cylinders are indeed very similar to the intensity profiles we have predicted. The images in section 4 are printed black-is-hot because they appear better when printed. To facilitate comparison of theoretical predictions with experimental results, we reproduce one of the plots from that section in figure 6, but shown for a white-is-hot image. Clearly, the plots in figures 5 and 6 are very similar indicating the validity of the theory.
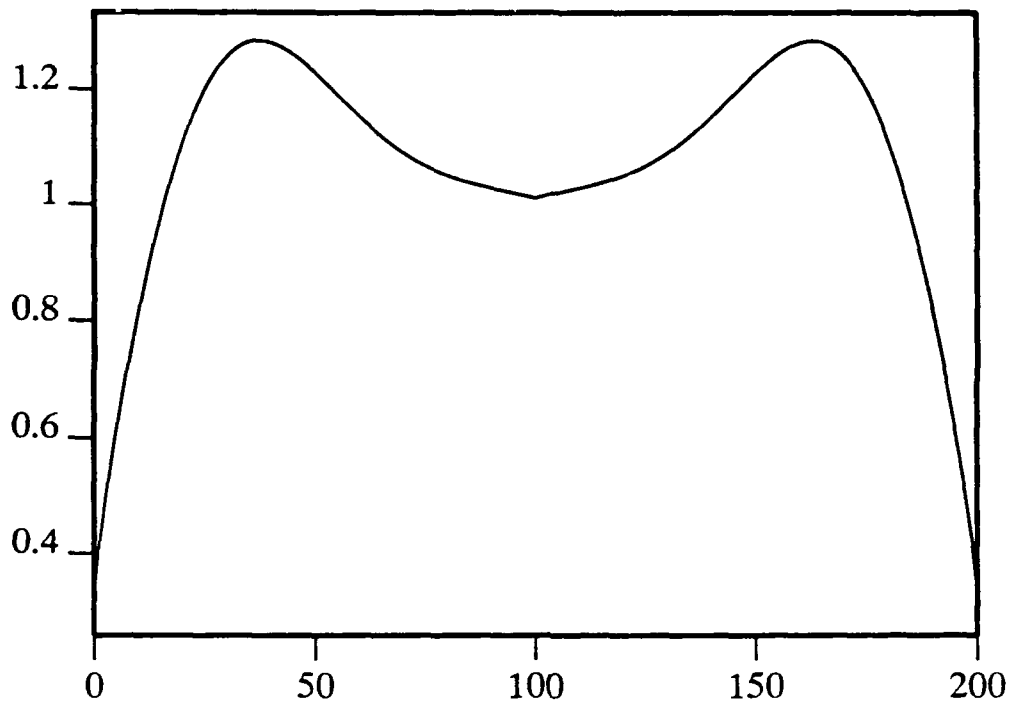
Figure 5: Predicted intensity profile of specularly reflecting concave non-Lambertian radiator
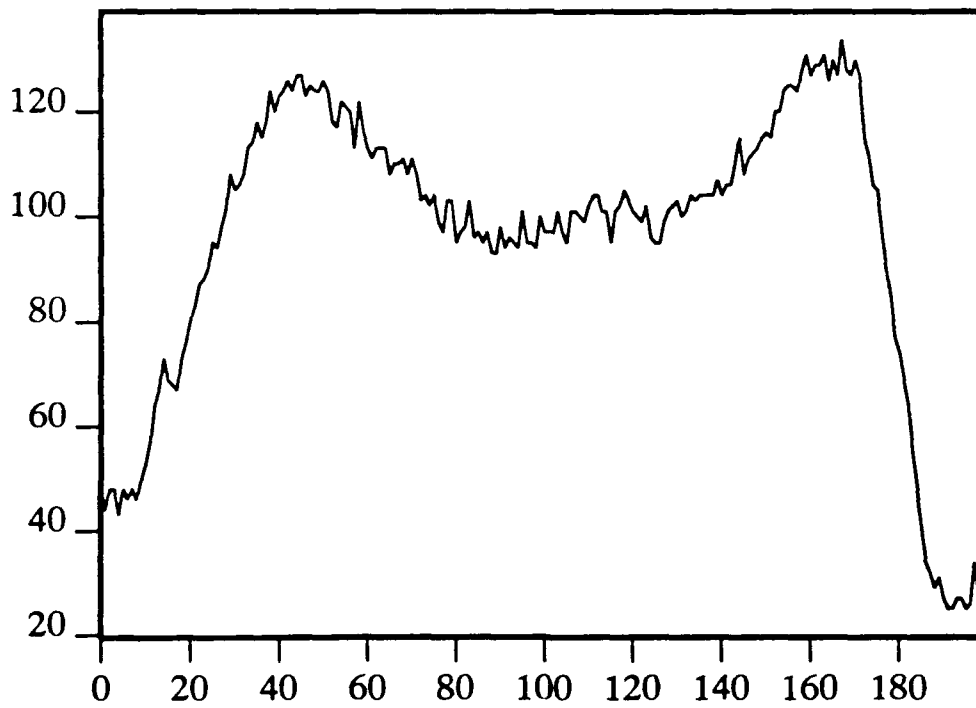

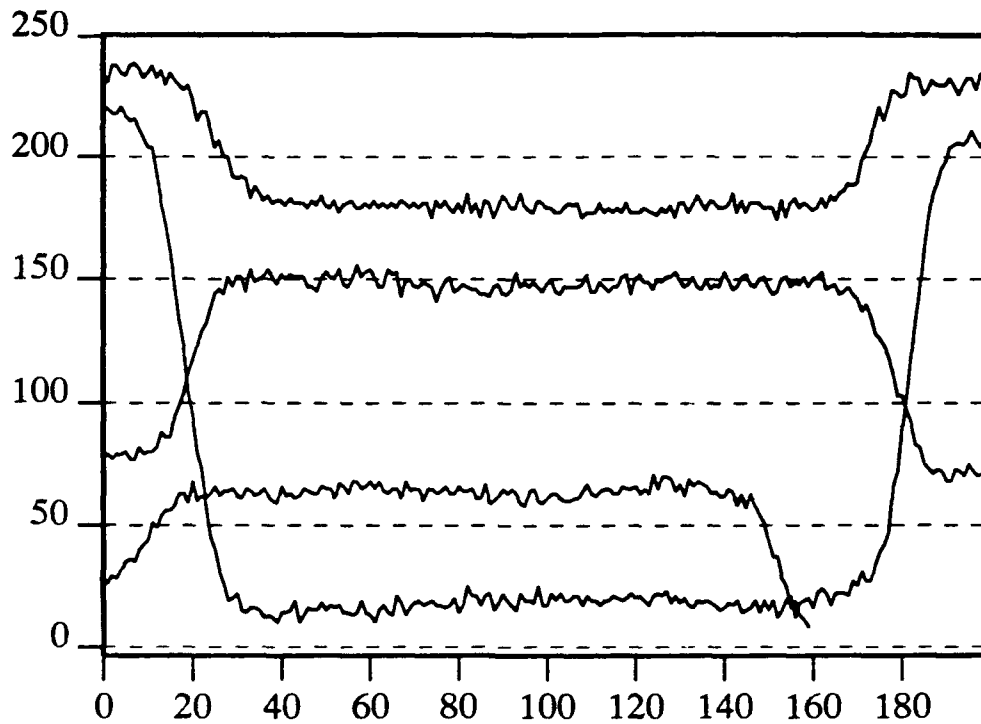Figure 6: Intensity cross-section of a non-Lambertian radiator

Figure 7: Cross-sections of convex black body

4 Experimental Results

The results presented in this section were taken from images taken using a thermal imager built in RSRE and Oxford University and described in [1]. The device is a chopped linear array of pyroelectric detector elements. The images were pre-processed to remove the effect of the dead elements in the array and to equalise differences between each of the detector elements. The pre-processing is described in [1].

We wished to examine the intensity profile across both concave and convex semi-cylinders of both black and non-black bodies. A target was made from a section of brass piping which could be viewed either as a concave cylinder from one side or a convex cylinder from the other and the surface was treated so that the reflective and emissive properties of both sides would be the same. Images were taken of the targets at different temperatures with both the convex side facing the imager and the concave side facing the imager. The surface of the target was then made black and the measurements were repeated.

Figure 7 shows a sample of cross-sections of the intensity of the target when made black from the convex side for a range of temperatures between $20°C$ and $46°C$. Figure 8 shows cross-sections of the intensity of the target when made black from the concave side for a similar range of temperatures. The intensity profiles of the two hotter objects in both figures have been offset with respect to the cold objects so that both can be displayed with reasonable resolution on the same axes. The background temperature for these experiments was approximately $31°C$.

Figures 7 and 8 show that the theory described earlier for black bodies does appear to be valid: the intensity profiles are very nearly flat for both concave and convex objects indicating that the irradiation at the imager is independent of the surface orientation *for black bodies*.

The intensity profiles of the images taken of the target before it was made black are very different from those of the black target. In this case, there was a specular reflective component in the radiation from the surface of the body. Figure 9 gives typical intensity profiles for the non-black targets. The lower line is the intensity profile across the image of the convex target at $46°C$ and the upper line is the intensity profile of the image of the concave target when it was at $41°C$. The difference between the two profiles is due to the mutual illumination effects discussed earlier and confirms the theoretical predictions.

5 Image recognition

In the previous section, we demonstrated that certain different object shapes and surfaces have characteristic intensity profiles. In this section, we will demonstrate how knowledge of these intensity profiles can be used to
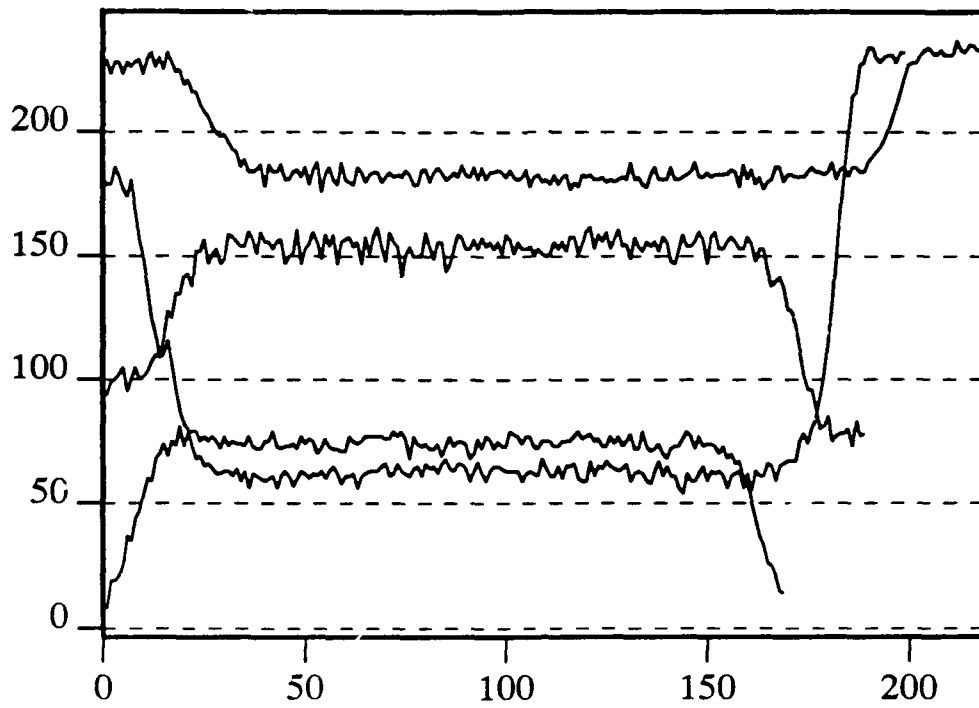
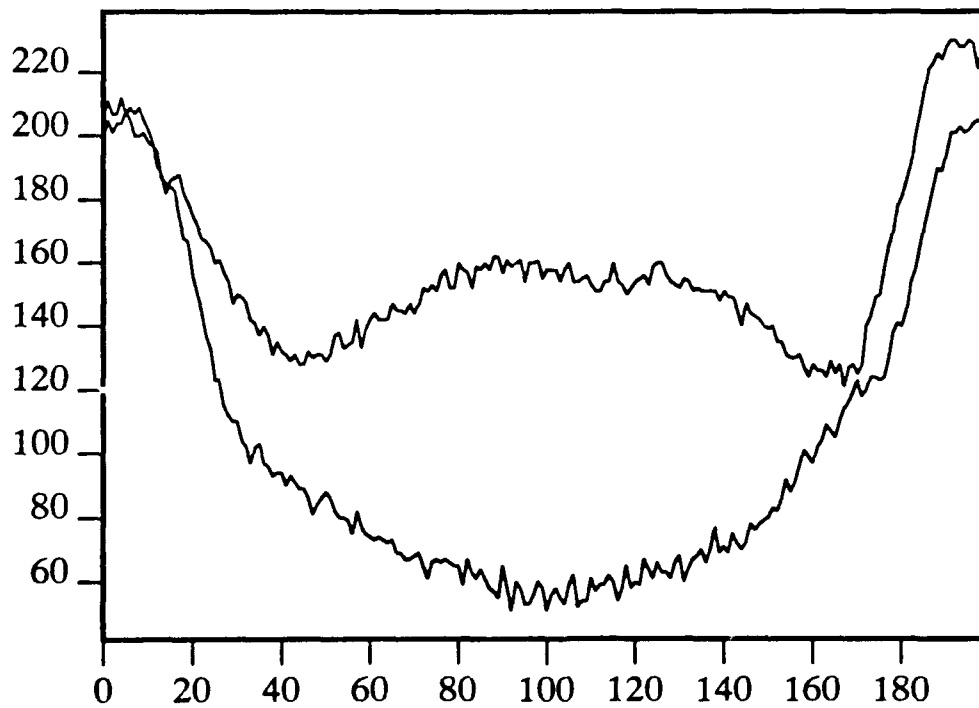Figure 8: Cross-sections of concave black body

Figure 9: Cross-section of convex (lower) and concave (upper) non-black bodies
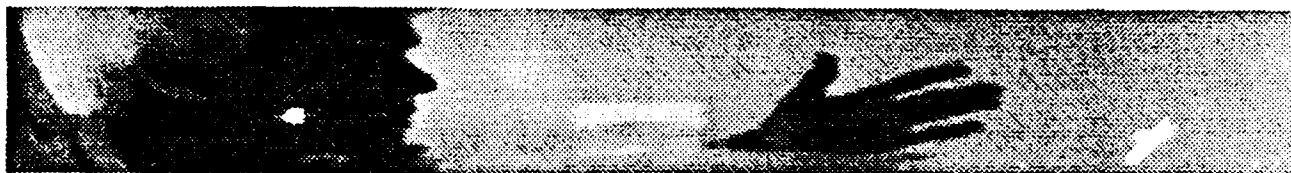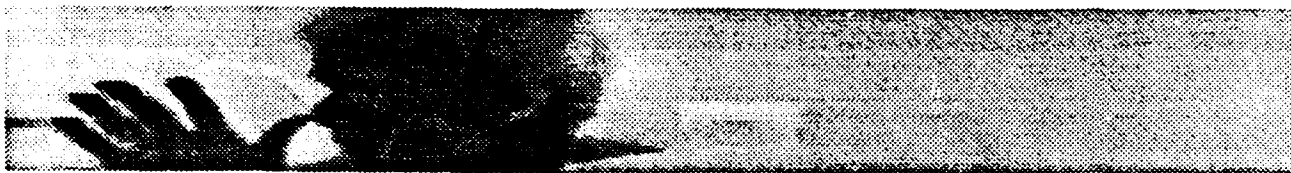
Figure 10: Image containing convex cylinder

Figure 11: Image containing convex cylinder

recognise the existence of a particular object.

A series of images was taken containing cool convex non-black cylinders along with other objects which were both warmer and cooler than the environment. Figures 10 and 11 are two typical examples. In both of these images, a black body cylinder at the same temperature as the non-black cylinder lies immediately above the cylinder indicating the position of the cylinder (just to the left of the hand in figure 10 and to the right of the head in figure 11).

The non-black body cylinder has a radiance pattern similar to that of the plot of the intensity of the convex body in figure 9, while the intensity profile of the black body is approximately constant. Figures 12 and 13 show horizontal intensity profiles of two lines of the image in figure 10. Figure 12 shows a cross section which crosses the non-black cylinder, while Figure 13 shows a cross section from a part of the image above the black cylinder.

The purpose of the demonstration described in this section was to identify cylinders in images using only information about their shape characteristics. Examining the plots in figure 12, and other cross-sectional plots, we decided that it would be possible to estimate the position of the cylinder by detecting the position of a "cylinder-like" profile in the one dimensional signal. The algorithm which is briefly described below was not designed to be useful (without modification) for any other problem: its purpose was to demonstrate the feasibility of object detection using intensity information from different surface properties within a body.

The first stage of the processing was to filter the image to reduce the amount of noise. This was done using a simple Gaussian filter. We removed the constant parts of the background by convolving the image with a simple edge detector and eliminating points with zero edge strength.

We then searched the remaining points for occurrences of pairs of edge gradients: a negative edge gradient separated from a positive gradient by a distance within a specified range. Once a negative edge gradient had been encountered, a search was made for a neighbouring positive edge gradient. Starting at a point beyond the maximum width of a cylinder, the pixel values were searched backwards until a positive gradient was found with an intensity value not too different from the intensity value of the point with the negative edge gradient. If such a point was found before the distance between the points became less than the minimum expected width of a cylinder, the edge was retained as a possible cylinder edge; otherwise the point was removed from the search space. A fairly generous size margin was permissible between the edges of the cylinder to allow for variations in mirror speed, distance of target from the imager etc..

Further constraints were then applied to the remaining set of possible candidates. A particular set of intensity values could only be classified as a cylinder if the intensity of all points between the negative gradient edge and the positive gradient edge in the smoothed image had an intensity which was lower than the higher intensity value of the surrounding edge points. Similarly as the characteristic cross section of intensity values from a particular type of cylinder would not vary greatly if the temperature of the cylinder fell within some reasonable range, a region in the image would not be classified as a cylinder unless the intensities of points between the two suspected cylinder boundaries were neither too far from nor too near to the average intensity value of the surrounding points.

Initially, the thresholds which were set on all the parameters mentioned were very weak. We found that using this algorithm, we could detect the required target with only a few false targets. By tightening the thresholds, it was possible to reduce the number of false targets reported. Figure 14 shows the target from figure 10 located with no false targets and figure 15 shows the target in figure 11 located, again with no false targets.
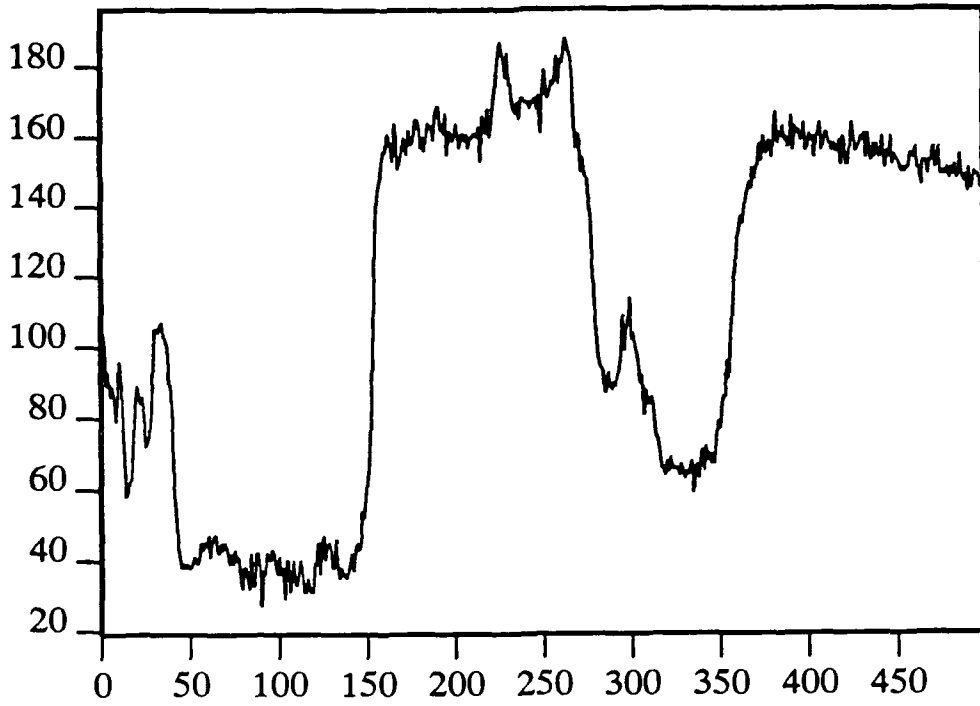
10

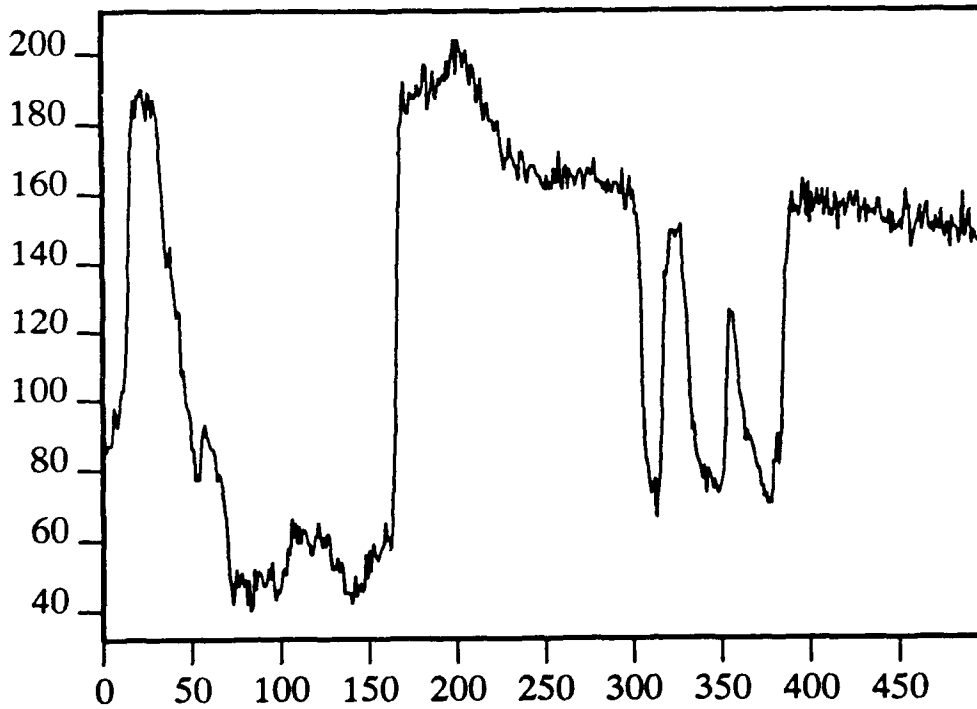Figure 12: Intensity cross-section from the image in figure 10

Figure 13: Intensity cross-section from the image in figure 10
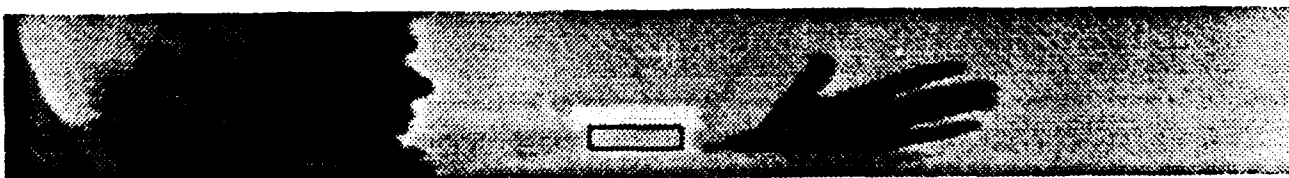

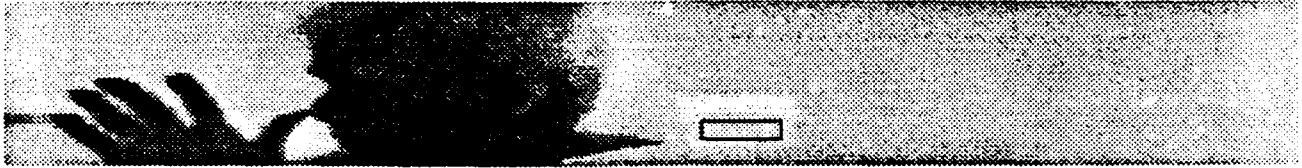Figure 14: Convex cylinder located
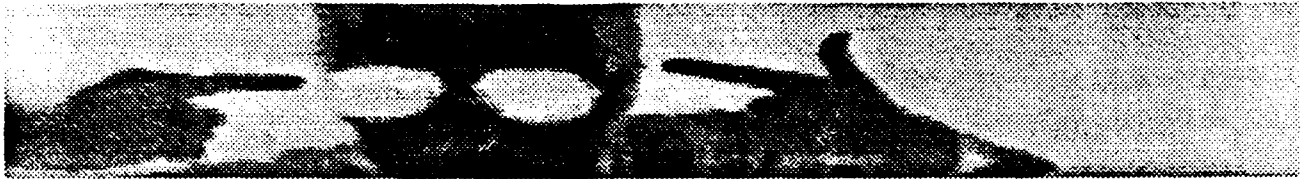
11

Figure 15: Convex cylinder located

Figure 16: Image containing convex cylinder

To demonstrate the robustness of the algorithm, we ran it on a variety of images with different background conditions and different target temperatures. To detect all targets in all of the images, it was necessary to weaken the thresholds again, but even with the weaker thresholds, only one or two false targets were reported. We found that over a reasonably large range of target temperatures, we could detect the target in the scene with no false target detection. Figure 16 shows an image where the target is harder to see (it is to the right of the person). In this image, using the same thresholds which were used to detect the targets in figures 14 and 15, the target was successfully detected, again with no false targets. The result is shown in figure 17.

We do not claim that this algorithm is anything more than an empirically derived set of instructions for detecting a very limited set of possible targets. It is important, however, since it demonstrates that internal infrared intensity values can be used to distinguish between shapes without recourse to temperature thresholding.

6   Conclusions

We have examined the image irradiance equation for infrared images. We have made predictions about the intensity profile across a simple geometric object emitting infrared radiation and have demonstrated that the profiles of real images are very similar.

We have highlighted the point that a knowledge of the infrared radiance pattern of an object can be used to characterise that object and we have shown experimentally that that characteristic profile can be used to distinguish the object from a cluttered scene.

7   Acknowledgements

The author acknowledges the support of RSRE and would like to thank Mike Brady of Oxford University for his assistance with this work.
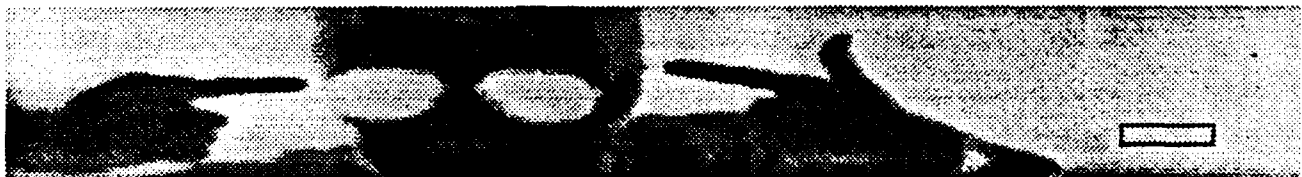

Figure 17: Convex cylinder located

8 Bibliography

References

[1] P.W. Foulkes. *Towards Infrared Image Understanding*. PhD thesis, Oxford University, December 1990.

[2] B.K.P. Horn. Understanding image intensities. *Artificial Intelligence*, 8(2):201–231, April 1977.

[3] Bui Tuong Phong. Illumination for computer generated pictures. *Communications of the ACM*, 18(6):311–317, 1975.

REPORT DOCUMENTATION PAGE

Overall security classification of sheet ....UNCLASSIFIED..

(As far as possible this sheet should contain only unclassified information. If it is necessary to enter classified information, the field concerned must be marked to indicate the classification eg (R), (C) or (S).

| Originators Reference/Report No.
MEMO 4464 | Month
MARCH | Year
1991 |
|---|---|---|

| Originators Name and Location
RSRE, St Andrews Road
Malvern, Worcs WR14 3PS		

Monitoring Agency Name and Location		

| Title
EXTRACTION OF SHAPE INFORMATION FROM PREDICTED IRRADIANCE PROFILES
IN INFRARED IMAGES		

| Report Security Classification
UNCLASSIFIED | Title Classification (U, R, C or S)
U |
|---|---|

Foreign Language Title (in the case of translations)	

Conference Details	

Agency Reference	Contract Number and Period

Project Number	Other References

| Authors
FOULKES, P W | Pagination and Ref
12 |
|---|---|

Abstract

In this paper, we address the problem of infrared image formation and derive an irradiance equation for simple infrared scenes. We consider the complications caused by mutual illumination of one or more bodies and indicate how the infrared irradiance equation can also be specified for more complex scenes.

The infrared irradiance equation we derive is solved in closed form for some simple geometries for both Lambertian and non-Lambertian surfaces. Experimental results from a variety of scene geometries compare favourably with the theoretically derived equations, indicating the validity of the theoretical analysis.

We describe how a knowledge of the formation of infrared images can be used to predict the image irradiance pattern of a particular object. We also show how, with a knowledge of the radiance properties and surface geometry of the object, it is possible to detect instances of that object in a scene.

Examples of successful object detection based on an understanding of the image irradiance are presented.

| Abstract Classification (U,R,C or S)
U |
|---|

Descriptors

Distribution Statement (Enter any limitations on the distribution of the document)

UNLIMITED

S80/48